Application of SEBAL approach and MODIS time-series to map vegetation water use patterns in the data scarce Krishna river basin of India

M.-D. Ahmad*, T. Biggs, H. Turral* and C.A. Scott****

*International Water Management Institute, Global Research Division, PO Box 2075, Colombo, Sri Lanka (E-mail: *a.mobin@cgiar.org*; *h.turral@cgiar.org*)

**International Water Management Institute, Regional Office for South Asia c/o ICRISAT, Patancheru, AP 502 324, India (E-mail: *t.biggs@cgiar.org*; *c.scott@cgiar.org*)

Abstract Evapotranspiration (*ET*) from irrigated land is one of the most useful indicators to explain whether the water is used as "intended". In this study, the Surface Energy Balance Algorithm for Land (SEBAL) was used to compute actual *ET* from a Landsat7 image of December 29, 2000 for diverse land use in the Krishna Basin in India. SEBAL ET_a varies between 0 to 4.7 mm per day over the image and was quantified for identified land use classes. Seasonal/annual comparison of ET_a from different land uses requires time series images, processed by SEBAL. In this study, the Landsat-derived snapshot SEBAL ET_a result was interpreted using the cropping calendar and time series analysis of MODIS imagery. The wastewater irrigated area in the basin has the highest ET_a in the image, partly due to its advanced growth stage compared to groundwater-irrigated rice. Shrub and forests in the senescence phase have similar ET_a to vegetable/cash crops, and ET_a from grasslands is a low 0.8 mm per day after the end of the monsoon. The results indicate that wastewater irrigation of fodder and rice is sufficient to meet crop water demand but there appears to be deficit irrigation of rice using groundwater.

Keywords Evapotranspiration; India; irrigation; remote sensing; river basin; water management

Water Science & Technology **Vol 53 No 10 pp 83–90** © IWA Publishing 2006

Introduction

Judicious management of precious land and water resources will be one of the biggest challenges of the 21st century. Both water and land resources are finite, but demand in various sectors is increasing. Irrigated agriculture, a major contributor to global food production, is one of biggest consumers of fresh water, accounting for about 70% of global diverted water resources. Considering the rapidly growing water demand for industries and domestic use, it is essential to use irrigation water more efficiently. Most of the large irrigation systems are located in arid to semi-arid regions where rainfall is much less than evaporative demand and agriculture is only possible with surface or groundwater irrigation. As a result, evapotranspiration is one of the largest components in the overall water balance in these regions. Therefore knowledge of actual evapotranspiration in irrigated river basins is essential for efficient management of scare water resources. Spatial patterns of evapotranspiration explain whether the water is used as "intended" or not.

Conventional methods to compute evapotranspiration are based on climate data (Allen *et al.* 1998). In these methods routinely collected climatic data are used to compute evapotranspiration (*ET*) for a reference crop of alfalfa (Wright and Jensen, 1972) or short uniform grass (Doorenbos and Pruitt, 1977) and then using an area-specific crop coefficient (K_c), crop water requirement is calculated for different growth stages of the crop under investigation. Cropped area and K_c are not known with certainty and general values from the literature are usually used to estimate *ET*. Such estimates may differ considerably from the actual evapotranspiration (ET_a), due to variations in planting dates, crop

doi: 10.2166/wst.2006.301

growth stages and root-zone moisture conditions. Moreover, conventional techniques provide point estimates and often it is not practically possible to capture all the spatial variation at broad scales such as river basins, which are increasingly recognized as the management unit for irrigation and other water uses.

Actual evapotranspiration can be estimated from satellite remote sensing (Engman and Gurney, 1991; Kustas and Norman, 1996; Bastiaanssen *et al.,* 1998, 2002; Kustas *et al.,* 2003). Such methods provide a powerful means to compute actual evapotranspiration from an individual pixel to an entire raster image. Emerging developments in the field of remote sensing make it possible to overcome information limitations on soil water status, the actual evaporative depletion and estimation of net groundwater use for agriculture (Scott *et al.,* 2003; Ahmad *et al.,* 2005). As surface energy balances and crop water stress are directly linked to agricultural water use, ET_a variations in space and time are thought to be highly indicative for the adequacy and reliability of irrigation as well as the equity in water use. This study demonstrates the application of satellite remote sensing for land use classification and ET_a estimation in a data scarce basin, the Krishna in India.

High-spatial resolution snapshots of ET_a using SEBAL derived from Landsat may be usefully supplemented by high temporal resolution satellite imagery such as MODIS. MODIS has been used to map vegetation phenology and cropping pattern in the Krishna Basin, and is used to put the Landsat SEBAL results in the context of the annual vegetation and cropping cycles.

Description of the study area

This research was conducted using Landsat7 ETM satellite imagery of December 29, 2000 covering a part of the Krishna basin, 77°30′ to 78°54′ E and 16°46′ to 18°4′ N, in southern India (Figure 1). The Krishna Basin is the fourth largest river basin in India in terms of annual discharge and fifth in terms of basin area. The climate of the basin is predominantly semi-arid. Annual average precipitation is 780 mm and approximately 90% of annual

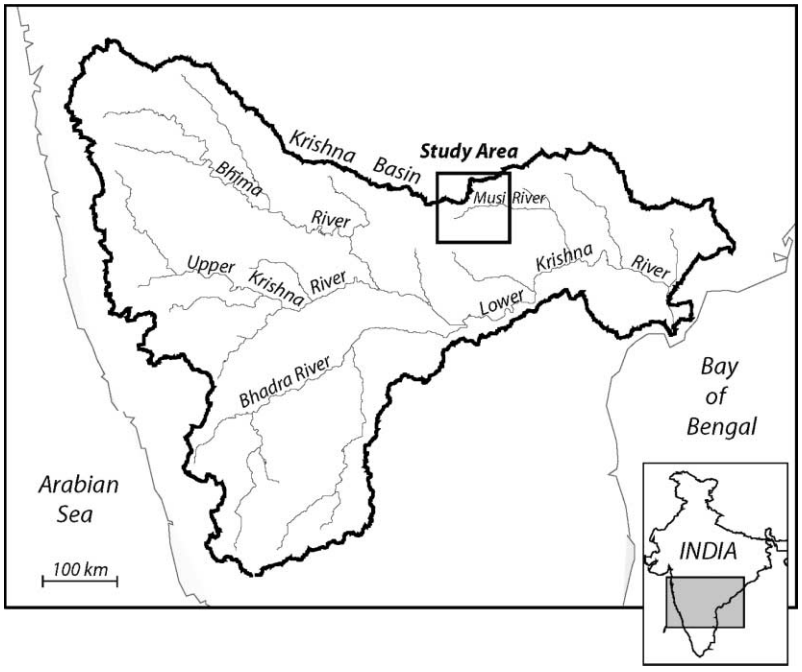

Figure 1 Location of study area in the Krishna Basin, India

precipitation occurs during the monsoon months of May–October. The Krishna basin has relatively diverse cropping patterns (Neena, 1998). Crops include rice, maize, sorghum, sugar-cane, millet, groundnut, and fodder grass. The area used for the SEBAL analysis has three major cropping regions: a vegetable and cash crop area on black vertsols soils to the west of the city of Hyderabad, a wastewater irrigated area downstream of Hyderabad, and tank and groundwater-irrigated rice on red alfilsol soils to the east and south of Hyderabad. The annual cropping cycle consists of three periods: kharif during the wettest monsoon months (mid June–mid December), rabi in the post-monsoon (mid December–April), and the dry season during the months with little rainfall (mid April–May).

Weather data on Dec. 29, 2000, summarized in Table 1, were obtained from ICRISAT agricultural meteorological station located in the vicinity of Hyderabad, India (latitude: 17.53° N, longitude: 78.27° E, altitude: 545 m). Using the Penman–Monteith approach, the reference crop *ET* is 3.5 mm per day under these climatic conditions at this location.

Materials and methods

In this paper, the Surface Energy Balance Algorithm for Land (SEBAL, Bastiaanssen *et al.,* 1998; Bastiaanssen, 2000) is used to compute ET_a from satellite imagery having visible, near infrared and thermal infrared bands. SEBAL computes a complete radiation and energy balance along with the resistances for momentum, heat and water vapour transport for each pixel. SEBAL is a well-tested and widely used method to compute ET_a (Bastiaanssen *et al.* 1998, 2002; Farah 2001; Tasumi *et al.* 2003).

Evaporation is calculated from the instantaneous evaporative fraction, Λ, and the daily averaged net radiation, R_{n24}. The evaporative fraction, Λ, is computed from the instantaneous surface energy balance at the moment of satellite overpass on a pixel-by-pixel basis:

$$\lambda E = R_n - (G_0 + H) \tag{1}$$

where λE is the latent heat flux, R_n is the net radiation, G_0 is the soil heat flux and H is the sensible heat flux. The latent heat flux describes the amount of energy consumed to maintain a certain crop evaporation rate. The surface albedo, surface temperature and vegetation index are derived from satellite measurements, and are used together to solve R_n, G_0 and H. The latent heat flux, λE, is the residual term of the energy budget, and is used to compute the instantaneous evaporative fraction, Λ:

$$\Lambda = \frac{\lambda E}{\lambda E + H} = \frac{\lambda E}{R_n - G_0} \tag{2}$$

The instantaneous evaporative fraction, Λ, expresses the ratio of the actual to the crop evaporative demand when the atmospheric moisture conditions are in equilibrium with the soil moisture conditions. The evaporative fraction tends to be constant during daytime hours; the H and λE fluxes, on the contrary, vary considerably. The difference between the instantaneous evaporative fraction at the moment of satellite overpass and the evaporative fraction derived from the 24-h integrated energy balance is marginal, and

Table 1 Weather conditions on Dec. 29, 2000 in the Krishna Basin as per record of ICRISAT meteorological station (latitude: 17.53° N, longitude 78.27° E)

Max. temp. C°	Min. temp. C°	Rel. humidity % 7.17 h	Rel. humidity % 14.17 h	Wind speed m/s	Actual sunshine h	Rain mm	Pan evaporation mm
27.4	10.2	90	34	1.44	9.6	0	4.8

may be neglected (Brutsaert and Sugita 1992; Crago 1996; Farah 2001). For time scales of 1 day or longer, G_0 can be ignored and net available energy ($R_n - G_0$) reduces to net radiation (R_n). For the daily time scale, ET_{24} (mm d^{-1}) can be computed as:

$$ET_{24} = \frac{86400 \times 10^3}{\lambda \rho_w} \Lambda R_{n24} \quad (3)$$

where R_{n24} (W m^{-2}) is the 24-h averaged net radiation, λ (J kg^{-1}) is the latent heat of vaporization, and ρ_w (kg m^{-3}) is the density of water.

Satellite imagery. The Landsat7 ETM image of December 29, 2000 was obtained from Michigan State University for the study area. For SEBAL analysis, visible, near infrared (NIR) and thermal infrared (TIR) bands are required; the band and sensor characteristics of Landsat7 ETM are presented in Table 2.

Using reflectance (R and NIR) and radiance (TIR) of this imagery, different surface parameters, NDVI, surface albedo, surface emissivity and surface temperature are derived. Then R_n, G_0 and H are solved using the semi-empirical relationship between these surface parameters. Finally ET_a is calculated from Equation 3 for all pixels in the image.

Results and discussion

Using the December 29, 2000 Landsat7 ETM image and routine meteorological data on temperature, humidity, wind speed and sunshine hours, pixel-based daily ET_a is computed by solving the surface energy balance using Equations 1, 2 and 3 for the study area (Figure 2). The ET_a map (Figure 2) clearly indicates spatial patterns of ET_a for various land use classes that include dry/barren land, native vegetation, agricultural crops and water bodies. The computed ET_a ranges from 0 to 4.7 mm per day. The highest value of ET_a is observed for water bodies and is in the same range as pan evaporation measured at the meteorological station located within the image (see Table 1).

There are large tracts of rocky/barren land with almost zero evaporation. Dry grasslands on black soils have the lowest ET_a. Some bare rocks occur in the scene, but these tend to be rather small (10–50 m diameter) and are surrounded by shrubs with relatively high ET_a, giving the rocky-shrub lands a higher ET_a than the grasslands. The average value of ET_a for the whole image is 1.6 mm per day. Irrigated fodder grass along the head reach of the Musi River, with no apparent water stress, evaporates at a maximum rate of 3.4–3.5 mm per day, almost the same as Penman–Monteith reference crop ET_0. This indicates that estimated values of ET_a from SEBAL are in good agreement with local field measurements for wet land surfaces.

To investigate inter- and intra-class ET_a variations for different land use classes in the processed image, ET_a statistics (Table 3) from 12 different land uses were calculated using 44 representative polygons delineated using data from field surveys and visual image interpretation (Figure 3). This allowed separation of land use types that were not easily separated in an image classification due to mixed spectral information and different

Table 2 Characteristics of visible and infrared bands of Landsat7 ETM used for SEBAL application

Satellite imagery	Spectral range (microns)	Spatial resolution (m)
Landsat7 ETM (8 bit radiometric resolution)	Band 3: R (0.630–0.690)	30
	Band 4: NIR (0.750–0.900)	30
	Band 6: TIR (10.400–12.50)	60

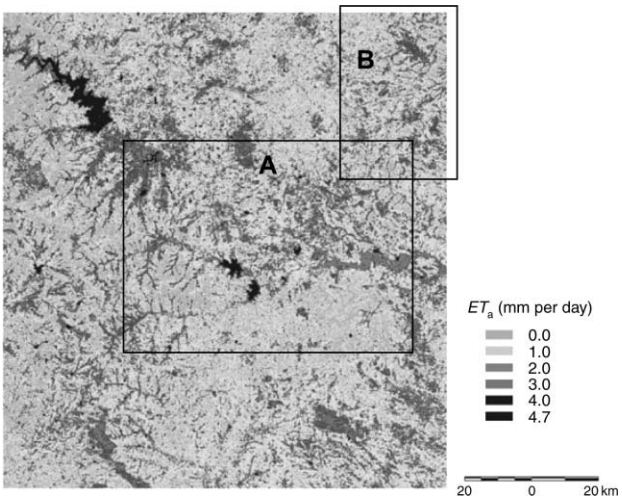

Figure 2 Actual evapotranspiration ET_a estimates using SEBAL for Landsat7 ETM imagery for Krishna Basin. December 29, 2000. A and B, areas selected for detailed comparison presented in Table 3

sources of irrigation, including riparian vegetation versus irrigated paragrass, groundwater irrigated versus wastewater irrigated areas, and plantations versus natural deciduous forest). For example, "natural vegetation" may include a mixture of rock, bare soil, and vegetation with different phonologies; a groundwater irrigated corridor contains a mosaic of different crops in different stages of growth; and the irrigated fodder paragrass corridor includes all rotations of the 30-day harvest cycle.

The wastewater irrigated area, including both paragrass and rice, has the highest ET_a in the image. Rice irrigated near tanks and by groundwater wells show ET_a values that are lower by 0.7 mm per day (20%). Rainfed crops have nearly the same ET_a as light-irrigated vegetable and cash crops (cotton). Plantations, mostly mangos, have the lowest ET_a of all crops at 1.9 mm per day. Grasslands have the lowest ET_a in the image, less than 50% of the next-lowest class. This is likely due to the shallow rooting depth of grass relative to the other vegetation types in the image. The low ET_a from plantations reflects the large spacing and low LAI of plantations relative to forests and green shrubs. Mango plantations have a field-estimated canopy cover of 15–25%, with bare soil between trees. Forests and shrubs tend to have higher canopy coverage and understory vegetation.

The interpretation of the ET_a values depends critically on understanding vegetation phenology and cropping cycle at the time of image acquisition. The 8-day

Table 3 ET_a variation for the dominant land use pattern in Krishna Basin

Land use class	Map code	Stage of growth	Mean mm/day	Std dev.	Coeff. of variation
Water bodies		–	4.45	0.21	0.05
Irrigated fodder paragrass	PG	Rotational	3.16	0.23	0.07
Wastewater-irrigated rice	WWRI	Begin second crop	3.32	0.24	0.07
Tank-irrigated rice	TNKR	Between crops	2.66	0.44	0.17
Groundwater-irrigated rice	GWR	Between crops	2.62	0.37	0.14
Vegetables and cotton	VEGCOT	End first crop	2.20	0.49	0.22
Rainfed grains	GRA	End first crop	2.50	0.26	0.10
Fruit plantations	MAN, VIN	End major crop	1.87	0.36	0.19
Forest (tree dominant)	FTRE	Mid-senescence	2.69	0.40	0.15
Shrubs-grassland	FSRB, SRB	Mid-senescence	2.52	0.36	0.14
Grassland	GRS	Mid-senescence	0.74	0.35	0.47
Urban	U	–	1.35	0.44	0.32

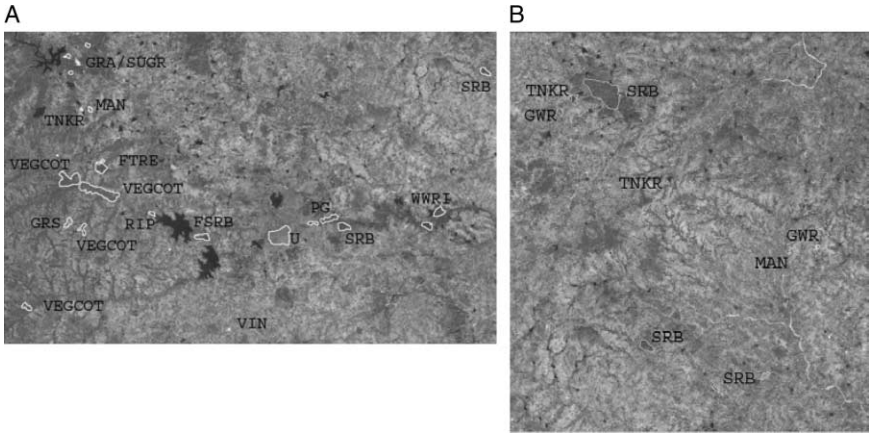

Figure 3 Polygons used to determine ET_a for representative land cover types. See Table 3 for names. A and B correspond to the frames in Figure 2

MODIS time-series of NDVI from May 2000–May 2001 shows the December 29, 2000 image in the context of the annual vegetation cycle for irrigated crops (Figure 4a) and rainfed areas (Figure 4b).

The December 29 image occurs after the monsoon growing season for rain-fed agriculture, rain-fed ecosystems and groundwater irrigated systems, and at the beginning of

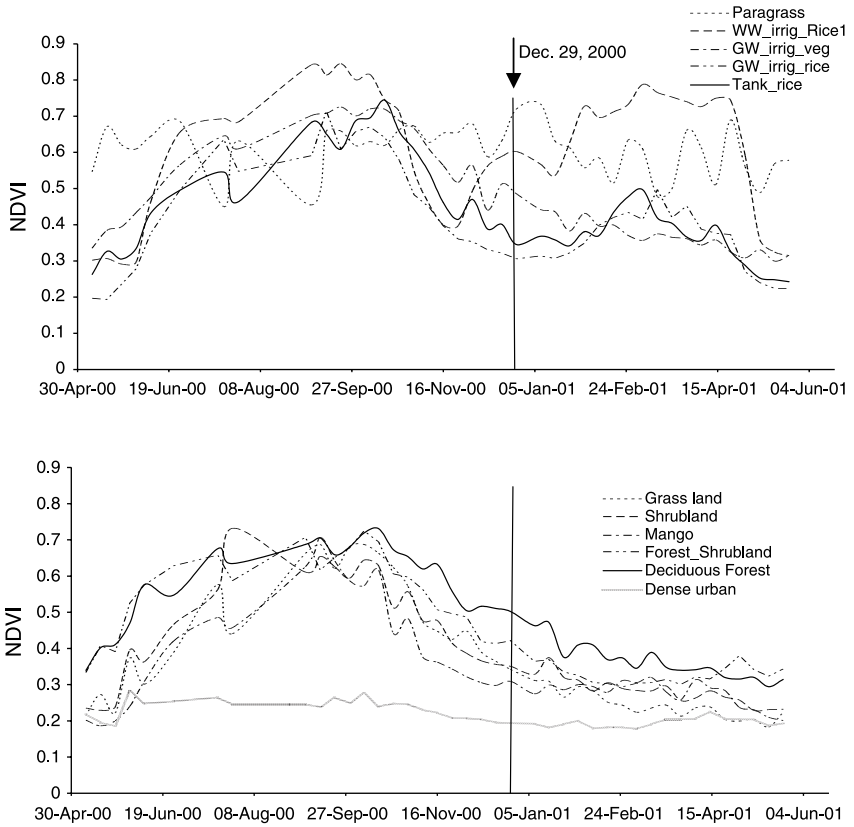

Figure 4 NDVI variation for different land use classes in Krishna Basin. (Based on 8-day MODIS time-series of NDVI from May 2000–May 2001)

the second cropping season for the wastewater irrigated area. Wastewater irrigated paragrass has perennially high NDVI that fluctuates relatively little due to the constant rotation of small patches on a 30-day harvesting cycle. The December image occurs between the monsoon and post-monsoon crops of groundwater/tank-irrigated rice, when NDVI is at a seasonal low and land cover is a mix of low stubble from recently harvested area, and flooded area in newly planted paddy. The wastewater irrigated area, by contrast, has an earlier onset of cropping and is in the middle of the development phase of the crop. Vegetative cover consists of 10–40 cm tall rice plants. Supplemental irrigated vegetable-cotton cropping is in the harvest and senescence phases.

The ET_a differences are related to both irrigation and vegetation phenology. Wastewater-irrigated rice has the highest ET_a of the vegetative areas in the image since it is a relatively homogenous cover of growing crop in the middle of its growth stage. The ET_a from paragrass is somewhat lower due to the rotational harvesting which results in a mosaic of grass in different stages of growth. ET_a from groundwater-irrigated rice is lower than ET_a from wastewater-irrigated rice. Both (crop growth stage and deficit irrigation) might cause the low ET_a in GW rice. Further field work to establish the causes for this is underway. Similarly, vegetable-cash-rain-fed cropping has a lower ET_a compared with wastewater-irrigated rice partly because the image occurs during the harvest and senescence phases of the cropping cycle. Interestingly, the grassland, which has the lowest ET_a of all classes in December, has nearly the same NDVI as shrubland and forest during the monsoon, suggesting that its low ET_a is mostly due to its rapid senescence after the monsoon season.

Conclusions

The purpose of this study was to demonstrate the application/utility of the SEBAL technique to map spatial variation in actual evapotranspiration for the data-scarce Krishna River basin. Data requirements for SEBAL processing include any satellite imagery with visible, near-infrared and thermal-infrared band such as Landsat, NOAA-AVHRR, MODIS and ASTER and routine meteorological measurement of air temperature, humidity, wind speed and sunshine duration. In this study a Landsat7 ETM image of December 29, 2000 was used to solve net radiation, soil heat flux and sensible heat flux components of the energy balance. Latent heat flux, the residual term of surface energy balance (Equation 1), was used to compute evapotranspiration for every 30 m × 30 m pixel. Another advantage of the SEBAL approach over conventional *ET* estimation methods is that it does not require detailed field information such as crop or land use type, sowing date, moisture status or area specific crop coefficients K_c, which are essential to compute ET_a using conventional techniques. However, critical to the interpretation of the SEBAL results is knowledge of cropping calendars; many of the differences between land cover types were due to differences in vegetation phenology, so the snapshot SEBAL results may not be representative of annual ET_a. A full time series of SEBAL would be needed to evaluate seasonal differences in ET_a from different vegetation types. The current snapshot demonstrates that ET_a from shrublands and forests is comparable to rain-fed and supplemental irrigated areas. Grasslands have very low ET_a as early as December, less than 2–3 months following the end of the monsoon, likely due to their shallow rooting depth relative to other vegetation types.

The combination of red, near infrared, and thermal infrared Landsat bands, which are used to calculate the surface energy balance and actual evapotranspiration from latent heat flux, and MODIS-derived land cover allow interpretation of the adequacy of irrigation. The study results indicate that perennially irrigated fodder grass and seasonal rice under wastewater irrigation downstream of a major urban center have the highest ET_a.

Groundwater and tank-irrigated rice, although at a different crop growth stage on the December 29, 2000 date of image acquisition, have lower evapotranspiration, suggesting reduced irrigation adequacy as corroborated by field experience. Given the lack of data on irrigation applications under any of the three principal sources of water—wastewater, groundwater, tanks—in the image, the remote sensing tools applied here offer a considerable advantage over time-consuming conventional ET_a estimation methods. However, interpretation of the results is greatly strengthened through field-based observations.

References

Ahmad, M.D., Bastiaanssen, W.G.M. and Feddes, R.A. (2005). A new technique to estimate net groundwater use across large irrigated areas by combining remote sensing and water balance approaches, Rechna Doab, Pakistan. *Hydrogeology Journal*, **13**(5–6), 653–664.

Allen, R.G., Pereira, L.S., Raes, D. and Smith, M. (1998). *Crop Evapotranspiration, Guidelines for Computing Crop Water Requirements*, FAO Irrigation and Drainage Paper 56, Food and Agricultural Organization of the United Nations (FAO), Rome, Italy.

Bastiaanssen, W.G.M. (2000). SEBAL-based sensible and latent heat fluxes in the irrigated Gediz Basin, Turkey. *Journal of Hydrology*, **229**, 87–100.

Bastiaanssen, W.G.M., Ahmad, M.D. and Chemin, Y. (2002). Satellite surveillance of evaporative depletion across the Indus. *Water Resources Research*, **38**(12), 1273, 1–9.

Bastiaanssen, W.G.M., Menenti, M., Feddes, R.A. and Holtslag, A.A.M. (1998). A remote sensing surface energy balance algorithm for land (SEBAL), part 1: formulation. *Journal of Hydrology*, **212–213**, 198–212.

Brutsaert, W. and Sugita, M. (1992). Application of self-preservation in the diurnal evolution of the surface energy budget to determine daily evaporation. *Journal of Geophysical Research*, **97**(D17), 18322–18377.

Crago, R.D. (1996). Conservation and variability of the evaporative fraction during the day time. *Journal of Hydrology*, **180**, 173–194.

Doorenbos, J. and Pruitt, W.O. (1977). *Crop Water Requirements*, Irrigation and Drainage Paper no. 24 (revised), FAO, Rome, Italy.

Engman, E.T. and Gurney, R.J. (1991). *Remote Sensing in Hydrology*, Chapman and Hall, London, UK.

Farah, H.O. (2001). Estimation of regional evaporation using a detailed agro-hydrological model. *Journal of Hydrology*, **229**(1–2), 50–58.

Kustas, W.P. and Norman, J.M. (1996). Use of remote sensing for evapotranspiration monitoring over land surfaces. *Hydrological Sciences Journal*, **41**(4), 495–516.

Kustas, W.P., Diak, G.R. and Moran, M.S. (2003). Evapotranspiration, Remote Sensing of. In: *Encyclopedia of Water Science*, Marcel Dekker, Inc., New York, pp. 267–274.

Neena, D. (1998). Inter-state variation in cropping pattern in India. *Indian Journal of Regional Science*, **30**, 57–69.

Scott, C.A., Bastiaanssen, W.G.M. and Ahmad, M.D. (2003). Mapping root zone soil moisture using remotely sensed optical imagery. *Journal of Irrigation and Drainage Engineering ASCE*, **129**(5), 326–335.

Tasumi, M., Trezza, R., Allen, R.G. and Wright, J.L. (2003). U.S. Validation tests on the SEBAL model for evapotranspiration via satellite. *ICID Workshop on Remote Sensing of ET for Large Regions*, Montpellier, France, 17 Sept. 2003.

Wright, J.L. and Jensen, M.E. (1972). Peak water requirements of crops in Southern Idaho. *Journal of Irrigation and Drainage Division, ASCE*, **96**(1), 193–201.